Applied Surface Science Advances 28 (2025) 100794

Contents lists available at ScienceDirect

Applied Surface Science Advances

journal homepage: www.sciencedirect.com/journal/applied-surface-science-advances

Full Length Article

Theoretical study of the adsorption of methyl formate on the MgO (100) surface

R.E. Ambrusi [a,b], J. Juan [a,b], J.M. Marchetti [c,*]

[a] Instituto de Física del Sur (IFISUR), CONICET, Av. L. N. Alem 1253, B8000CPB-Bahía Blanca, Argentina
[b] Departamento de Física, Universidad Nacional del Sur (UNS), Av. L. N. Alem 1253, B8000CPB-Bahía Blanca, Argentina
[c] Faculty of Science and Technology, Norwegian University of Life Sciences, Drøbakveien 31, 1430 Ås, Norway

ARTICLE INFO

Keywords:
MgO
Methyl formate
DFT
Catalysis
Adsorption

ABSTRACT

A density functional theory study was performed to understand the interactions of the methyl formate molecule with the MgO (100) surface. In this context, the adsorption mechanisms of the molecule were investigated, with a focus on its stability on the substrate, the geometric structure of the system, and the interactions between the molecule and the surface. Two main stable configurations with approximately the same adsorption energy (about 0.47 eV) were found. The first configuration involves the oxygen of the carbonyl group on the Mg top site, while the second involves the remaining ester group oxygen on the same site. It is important to emphasize that each configuration interacts in different proportions in chemical and physical mechanisms, and with different bond participation. To comprehensively understand these phenomena, a systematic study was conducted, incorporating energy calculations, density of states, and charge and density difference analyses. Furthermore, chemical descriptors such as overlap population and bond order were employed to supplement the electronic results through a qualitative analysis of the main bonds.

1. Introduction

Magnesium oxide (MgO) has been identified as a material of interest for a variety of applications due to its unique dielectric, optical and isolating properties [1–4], which have made it emerge as a promising candidate in the field of ceramic materials synthesis. Additionally, MgO has gained attention as a potential alternative to conventional solar and fuel cells for electricity generation through water splitting, underscoring its significance in energy conversion [5]. It is established that several reactions of catalytic interest such as dehydrogenation of alcohols, aldol condensation, which involves heterolytic bond breaking, are favored by the MgO surface [6–8]. This feature is believed to be a consequence of the MgO catalyst's basicity, which originates from the basic character of the surface oxygen anion that predominates over the acid character of the Mg^{2+} cation [9,10].

MgO has been positively tested for the valorization of fatty acids and triglycerides intro biodiesel or Fatty Acid Alkyl Esters (FAEE) in particular for FAME (Fatty Acid Methyl Esters) [11–13]. These reactions have been under studied due to their high promising avenue for production petroleum fuel based substitutes with great beneficial environmental benefits such as biodegradability, lower CO and CO_2 emission, no sulfur contamination, among others [14–16]. Furthermore, they are key placers to achieve international agreements, such as the reductions of emissions by 2030 and it is envisioned that by 2050, they will be eliminated [17–18].

Biodiesel can be produced through the esterification of fatty acids or by transesterification of triglycerides, with the latter process being catalyzed by both homogeneous and heterogeneous catalysts [11–15]. Traditionally, homogeneous catalysts has been used homogeneous catalysts, such as KOH or NaOH, which present the disadvantage of requiring a refine feedstock [19,20]. Due to the need to use lower quality feedstocks, heterogenous processes have been developed and optimized [21–23]. Among them, solid alkaline earth metal oxides such as MgO and CaO [24,25] are gaining more and more relevance.

Several works have shown the advantages of using MgO for the production of biodiesel [26–30].Among those works, the work from Di Serio [31] has shown that a yield of 92 % using a 12:1 methanol to oil molar ratio with 5.0 wt. % of the catalyst in 1 h when using MgO, while the work of Eladeb [30]where MgO was used with a concentration of 3 wt % at 65 °C with a molar ratio of 9:1 of methanol allowing a yield of 92

* Corresponding author at: Norwegian University of Life Sciences, Faculty of Sciences and Technology, Norwegian University of Life Sciences, Drøbakveien 31, 1432 Ås, Norway.
E-mail address: jorge.mario.marchetti@nmbu.no (J.M. Marchetti).

https://doi.org/10.1016/j.apsadv.2025.100794
Received 22 April 2025; Received in revised form 31 May 2025; Accepted 14 June 2025
2666-5239/© 2025 The Author(s). Published by Elsevier B.V. This is an open access article under the CC BY license (http://creativecommons.org/licenses/by/4.0/).

% after 3 h of reaction. In addition, other researchers such as Chouhan et al., Singh et al., Gadore et al. and Patil et al. [24,25,32,33]. have presented the benefits of using metal oxides catalysts over conventional heterogeneous materials.

Theoretical works concerning the production of biodiesel have been evaluated using hydrotalcites heterogeneous catalysts [34]. Furthermore, the reaction mechanism involved in the alkaline-catalysed transesterification of pentylic acid triglyceride, which is the method generally adopted for large-scale biodiesel production, was studied employing Density Functional Theory (DFT) in both the gas phase and in solution [35]. A combination of experimental and theoretical works has been performed to analyze different aspects of the reaction steps involving products or reagents related to biodiesel production on MgO as a heterogeneous catalyst. For instance, Belelli et al. [36] have modeled the interactions of methyl oleate FAME with stepped MgO surface using a shorter saturated methyl ester containing three carbon atoms in the acyl group, achieving that the most stable adsorption is through the $C = O$ group where the Mg of the surface and O of the molecule has the lowest bond distance with slight changes in the FAME internal geometry with respect to the free molecule. Cornu et al. [37] performed a DFT and experimental study for the transesterification of esters using ethyl acetate with methanol on MgO defective surfaces, proposing plausible mechanisms. In that work, they analyzed the impact of the basicity of solids and linked it with the reactivity of the surface in gas and liquid phases. In a related study, Dicosimo et al. [38] conducted experimental and theoretical analyses of basic catalysis on MgO, focusing on the catalytic properties of active sites. Their approach involved DFT calculations of the adsorption and activation of alkyl esters up to five carbon atoms, simulating long carbon strings of FAME on various defect types, including Mg and O apical corner and edge sites. However, the study focuses on the glycerolysis of FAME to produce mono-, di- and triglycerides on MgO. In the theoretical simulations, using a cluster approach, calculations were performed with the aim to establish the intervening species stability at different sites to comprehend better the chemical mechanisms for FAME activation and the obtained experimental results, but without studying the electronic properties of the systems. Additionally, FAME adsorption on defective MgO surfaces was analyzed by DFT to study monoglyceride synthesis by glycerolysis of methyl oleate on MgO surface [39].

A study by Man et al. [40], investigated how methyl acetate and methanol are activated on a MgO(100) with a step defect catalyst surface. This study aimed to gain a better understanding of how certain reactions work at the atomic level. However, the non-defected MgO surface has not been the focus of sufficient attention about FAME adsorption. In addition, the work of Montero et al. [41].shows the adsorption of different molecules involved in biodiesel production over a nanosized material of MgO. The authors found out that the structure (100) was suitable for physisorption of methanol. In addition, it was found that the (100) structure was optimized for the adsorption of ester molecules, similarly to the work done by Cornu et al. [37]. Similarly, a theoretical study of processes related to biodiesel production on non-defected surfaces has already been performed on a CaO surface by Orazi et al. [42], that studied the ethanol adsorption on a CaO(001) surface at low coverages. Additionally, Bechthold et al. [43] have conducted a DFT study of formic acid adsorption on the same surface. Furthermore, FAME adsorption using ethyl formate molecules was performed on CaO(100) [44] to understand the adsorption on the catalyst surface, which is essential for optimizing the reaction conditions and controlling the amount of solvent used in the reaction.

This work represents, to the best of our knowledge, a novel attempt to understand at the atomic level the interaction between methyl formate and a MgO (100) surface without defects because all previous surface studies over MgO, especially on MgO (100), has been done with defects and other molecules. Methyl formate is the smaller ester to be produced bio-based and a systematic study of the adsorption geometry, stability and electronic structure was conducted in detail. Due to its simplicity in geometry and structure it is suitable to fully understand the functional group interactions with the surface and how it can be extrapolated to longer chains and therefore more complex molecules. Furthermore, a qualitative bonding analysis was included to reveal the main interactions and mechanisms for the adsorption. The molecule used in the calculations shares the same oxygen functional groups as the biodiesel product, showing the importance of investigating this catalyst. This approach had not been analyzed before and would lead to interesting results about MgO as a biodiesel catalyst. Consequently, the proposed model will facilitate the determination of the catalytic activity of a perfect MgO surface for this particular process.

2. Computational method

The calculations were carried out using the Vienna Ab Initio Simulation Package (VASP) [45,46], which enables the analysis of various material properties at the atomic scale based on DFT. A plane-wave basis set and a periodic supercell approach were employed to variationally solve the Kohn–Sham (K-S) equations. Core electrons were represented using the Projector Augmented Wave (PAW) method [47,48], and exchange-correlation interactions were modeled with the Generalized Gradient Approximation (GGA) using the Perdew, Burke, and Ernzerhof (PBE) functional [49]. The K-S wave functions of the valence electrons were expanded with a kinetic energy cutoff of 800 eV for the entire plane-wave basis set. A grid centered at the gamma point was used to sample the k-points with the Monkhorst–Pack scheme [50].

Geometry optimizations, including all the system atoms, were performed via total energy minimization of the supercell using a conjugate gradient algorithm to relax the ions [51]. The convergence criterion was set to 10^{-4} eV for electronic energy and 0.01 eV $Å^{-1}$ for the forces on each ion. Brillouin zone integrals were solved using a $7 \times 7 \times 1$ k-point grid, and Gaussian smearing was employed to represent the partial occupation of electronic states near the Fermi level, with a small smearing width of 0.05 eV. The forces of van der Waals (vdW) were accounted for using atomic pairwise corrections based on Grimme's DFT-D2 method [52].

We followed the procedure described by Tosoni and Sauer for the adsorption of CH_4 on MgO(001) [53]. We chose Grimme's DFT D2 dispersion correction over newer schemes because it is based on the literature and our experience. Freire et al. provided a detailed comparison of the performance of van der Waals dispersion functionals for water and ethanol adsorption on transition metal surfaces [54]. Yuan et al. studied the effects of van der Waals dispersion interactions on adsorption, catalysis, and tribology on metals [55]. Rehak et al. examined the performance of nine commonly used methods for including dispersion interactions in DFT [56]. The comparison included three different parametrizations of damped $1/R_n$ terms ($n = 6$, 8, etc.) added to the DFT energy (Grimme's D2 and D3 parameterizations as well as that of Tkatchenko and Scheffler (TS)), three different implementations of the many-body dispersion approach (MBD, MBD/HI and MBD/FI), the density-dependent energy correction, called dDsC, and two ''first generation'' van der Waals density functionals, revPBE-vdW and optB86b-vdW. This work analyzed the adsorption of carbon monoxide, as well as that of monolayers of methane and ethane, on MgO(001). The authors concluded that D3 or TS are not an improvement compared to D2, neither with PBE nor with B3LYP, for the eight cases of adsorption on flat oxide surfaces and in nanopores of MOFs and zeolites. Our recent study of Ni/SWCNT shows that there are no differences when using D2 or D3 methods [57]. It is important to note that findings may differ in other systems.

The surface structure was represented through a slab model of 4×4 bulk cells, and the size of the slab and vacuum were chosen to avoid interactions of the molecule in the perpendicular and lateral directions. Vectors in the y and z directions of 11.84 Å are parallel to the surface, and images of a vacuum of 30 Å in the x direction were employed perpendicular to it. The supercell contains 80 O and 80 Mg atoms with

five layers, and for all calculations, the top three layers were relaxed while the two lower ones remained fixed according to the bulk structure.

The adsorption of the molecule on the MgO surface was calculated using the following Eq. (1):

$$E_{ads} = E[MF/MgO] - E[MgO] - E[MF] \quad (1)$$

where E(MF/MgO), E(MgO) and E(MF) are the total energies of the methyl formate molecule adsorbed on the MgO (100) surface, and the isolated surface and molecule, respectively. A negative value of the adsorption energy indicates stable adsorption of the molecule on the oxide surface. A Γ-point calculation was performed for the relaxed isolated molecule structure in a cubic box with a side length of 20 Å to calculate the unadsorbed molecule energy.

Based on previous works [58,59], the adsorption energy can be expressed in term of DFT contribution and dispersion effect part, as in Eqs. (2) and 3:

$$E_{ads_DFT} = E_{DFT}[MF/MgO] - E_{DFT}[MgO] - E_{DFT}[MF] \quad (2)$$

$$E_{ads_vdw} = E_{vdw}[MF/MgO] - E_{vdw}[MgO] - E_{vdw}[MF] \quad (3)$$

where, E_{ads_DFT} and E_{ads_vdw} are the adsorption energies contributions obtained with the DFT total energies (solving Kohn sham equations) and the semiempirical dispersion energies respectively. According to these expressions $E_{ads} = E_{ads_DFT} + E_{ads_vdw}$.

The charge distribution was analyzed before and after molecule adsorption by computing the electronic charges on selected atoms using Bader analysis [60]. Additionally, to provide complementary information on the spatial charge distribution, the charge density difference ($\Delta\rho$) isosurface was calculated as follows:

$$\Delta\rho = \rho_{MF/MgO} - \rho_{MgO} - \rho_{MF} \quad (4)$$

In this equation, $\rho_{MF/MgO}$ represents the charge density of the system formed by the molecule adsorbed on the MgO (100) surface, while ρ_{MgO} and ρ_{MF} indicate the charge densities of the surface without the adsorbed molecule and the isolated molecule, respectively.

To gain a more comprehensive understanding of the electronic structure and the primary interactions between the molecule and the surface, the density of states (DOS) and the partial (or projected) density of states (PDOS) were calculated. Furthermore, a qualitative study of the key bonds was conducted using the overlap population (OP) and bond order (BO) concepts, as implemented in the DDEC6 method [61–63].

3. Results and discussion

3.1. The mgo bulk and (100) surface

The MgO crystal structure is analogous to rock salt, with a cubic Fm-3 m space group configuration. Each Mg^{2+} ion is bonded to six equivalent O^{2-} ions, and each O^{2-} ion is bonded to six equivalent Mg^{2+} ions. These ions are arranged in octahedra, as illustrated in Fig. 1(a). The calculated lattice parameter was found to be 4.19 Å, a value that aligns closely with the range of 4.23–4.26 Å reported in theoretical publications [64,65] and with experimental lattice parameters of 4.20 and 4.21 Å [65–67]. Fig. 1 also illustrates the supercell and slab model employed for the calculations.

As previous work [68] clearly shows, the (001) crystal plane is the most stable of the (111), (110) and (001) planes, with a lower surface energy of 1.37 J/m^2. In this work, we have chosen to study the (100) surface because it belongs to the same crystallographic family as the (001) plane. DFT calculations and surface science experiments consistently show (100) as the lowest energy and most stable surface for MgO. Experimental measurements and density functional theory (DFT) calculations using the PBEsol functional report surface energies in the range of 0.99 to 1.04 J/m^2 for MgO(100) [69]. The MgO (100) surface has been previously studied in other works for the adsorption of small molecules [70,71], but to the best of our knowledge, the methyl formate was not previously studied on this surface. In these works, four layers were used because no large relaxations of the surface occurred. Nevertheless, in the present work, calculations were performed with five layers instead to ensure that this parameter is well set. In addition, the study of this system could allow to compare the adsorption of other ester (ethyl formate) and other surface with the same crystal structure and different cation (CaO) [43].

To validate the proposed bulk structure and how the used effective potentials reproduce the electronic behavior, the DOS of the bulk

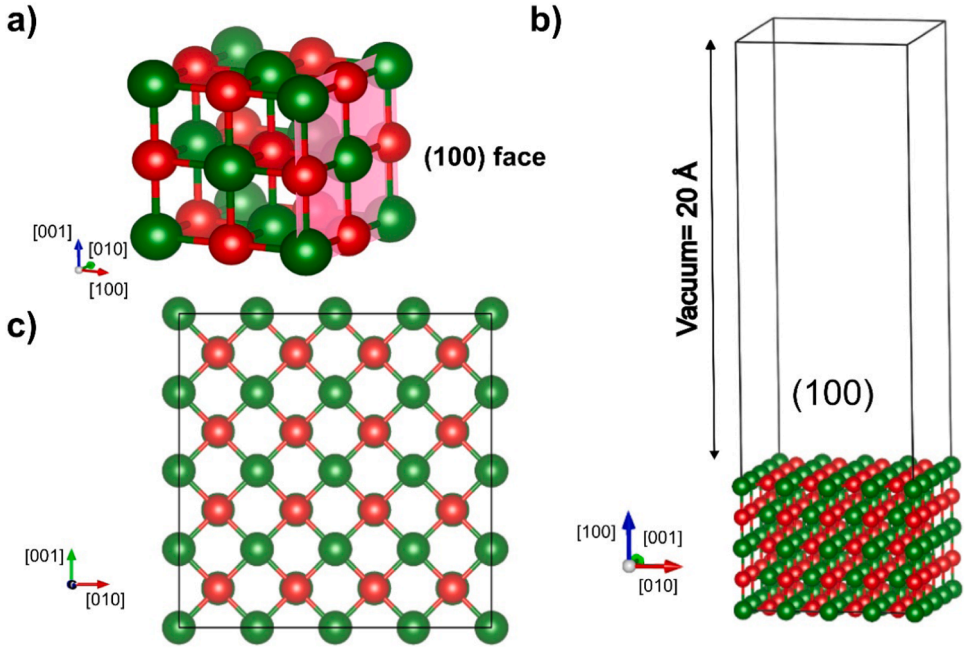


Fig. 1. Optimized structures for MgO bulk and (100) surface; (a) bulk structure, (b) slab model for the (100) surface, (c) top view of the surface. Green and red spheres represent Mg and O atoms respectively.

structure was calculated. The total DOS (TDOS) and the PDOS were differentiated, as illustrated in Fig. 2. The latter was performed on selected atoms or the molecule and specific atomic orbitals (referred to as on-site projection).

As illustrated in Fig. 2(a), the total density of states for the valence and conduction bands exhibits the conventional form characteristic of MgO, as observed in previous studies [68,70,71]. The band at lower energies is predominantly attributed to O atoms, while the other valence band, situated close to the Fermi level, is associated with O and Mg states. As can be observed in Fig. 2(b), the first one is related with O s states, while the second has contributions of Mg s and p states and O p states, with a major contribution of the latter. The results observed for the O projected states were in concordance with many theoretical results, including those of Avdeev et al. and Rodriguez et al. [70–72]. Additionally, the Mg s states contribution to the upper valence close to the Fermi level was observed by Rodriguez et al. through ab initio calculations [70,71].

Regarding Mg states, they are hybridized, which is not the case for O, which has separated s and p states. Finally, d states do not contribute to either O or Mg. Similar results were obtained for CaO bulk, where the O 2p band is close to the Fermi level, but with a different form, and the O 2 s orbital is approximately at −15 eV. However, the behavior of Mg states is quite different to that of Ca states, as previously reported by Orazi et al. [42]. This is because the Ca atom presents mainly a p band at approximately −19 eV, instead the Mg has a hybridized sp band close to the Fermi level, between −5 and 0 eV. At energies above 5 eV, Ca has unoccupied d orbitals on CaO, while in the case of Mg, there are sp unoccupied states in that range with no participation of Mg d orbitals.

According to the DOS, the band gap value is approximately 5 eV. It is important to note that this value is overestimated; however, it does align closely with the values of 4.43 and 4.45 eV obtained in other theoretical calculations using the GGA approximation [73,74].

The average valence states charge obtained with Bader method for Mg and O are 1.781 e and −1.780 e respectively, which are reasonable values close to the expected ones of +2e and −2e.

3.2. Geometric structure and stability of the methyl formate adsorption on mgo (100)

In Fig. 3, the two most stable configurations achieved after relaxation for methyl formate (MF) adsorption on the MgO (100) surface are shown. Fig. 4 represents a cutout of these structures with the main atoms labeled to be employed for geometrical, electronic and bonding analysis in this and the following subsections.

After a careful evaluation of the different tested sites and configurations for methyl formate adsorption on the MgO (100) surface, two most stable final configurations were detected, as previously stated. The first configuration (1) involved the oxygen of the carbonyl group on the Mg top site (see Fig. 4(a)), and the second configuration (2) involved the remaining ester group oxygen on the same site (see Fig. 4(b)). The adsorption energy, rounded to two decimal places, is 0.47 eV for both configurations, indicating a physical-chemical interaction with a mixed contribution of chemical and dispersion interactions. However, the mechanism is not the same for each configuration. For configuration 1, of –0.474 eV, the chemical and dispersion interactions have a similar contribution with 51 and 49 % of the total adsorption energy. In configuration 2, with an energy of −0.466 eV, the adsorption process is dominated by dispersion forces, with a contribution of 73 %. These energies are approximately 39 % of the adsorption energy obtained for ethyl formate on CaO (001) surface [44]. We consider that this difference occurs because of the variation in the surface basicity; the CaO surface being more basic. Recent calculations of ethyl acetate adsorption on MgO(110) facets and defect sites suggest binding occurs via a strong Lewis acid-base adduct [37], with the ester carbonyl coordinating through its oxygen to unsaturated Mg^{2+} cations in defective surfaces. Therefore, Mg behaves as a Lewis acid on the MgO (100) surface.

It is clear that the major contribution of adsorption dispersion energy for configuration 2 is related to the fact that the molecule's disposition is parallel, containing more atoms closer to the surface and allowing long-range interactions, such as physical dispersion interactions, that can be significant up to 3 Å [59,75]. Despite the fact of being the same site on the surface (Top of Mg), the molecule in each configuration interacts chemically through different oxygen atoms, being apparently slightly higher by the oxygen of carbonyl group (Config. 1). Further analysis of

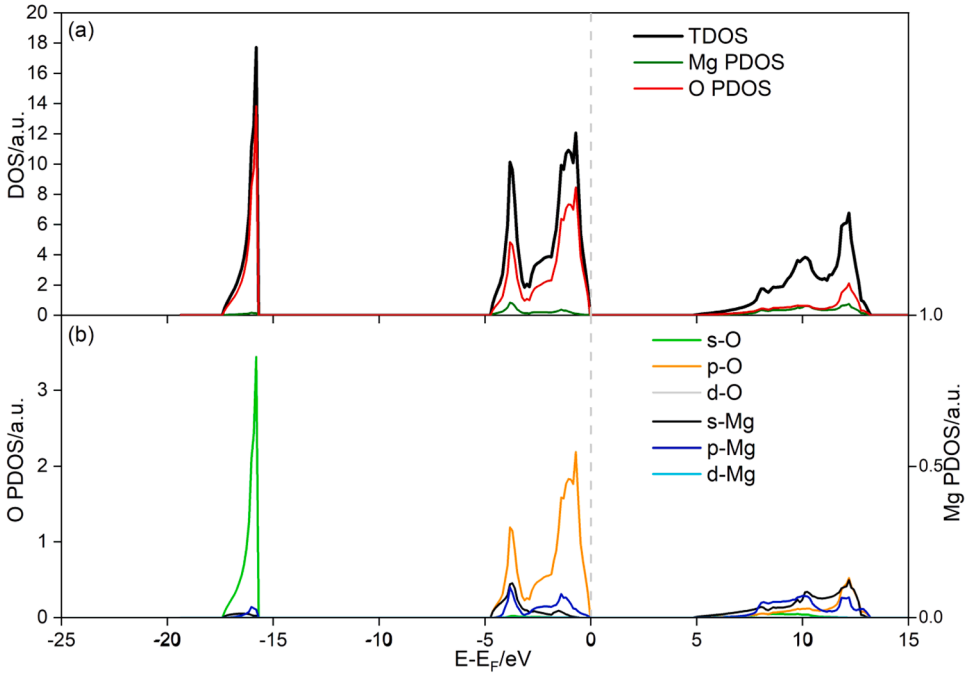


Fig. 2. DOS of the optimized MgO bulk; (a) TDOS and PDOS (on atoms), (b) PDOS (on orbitals).

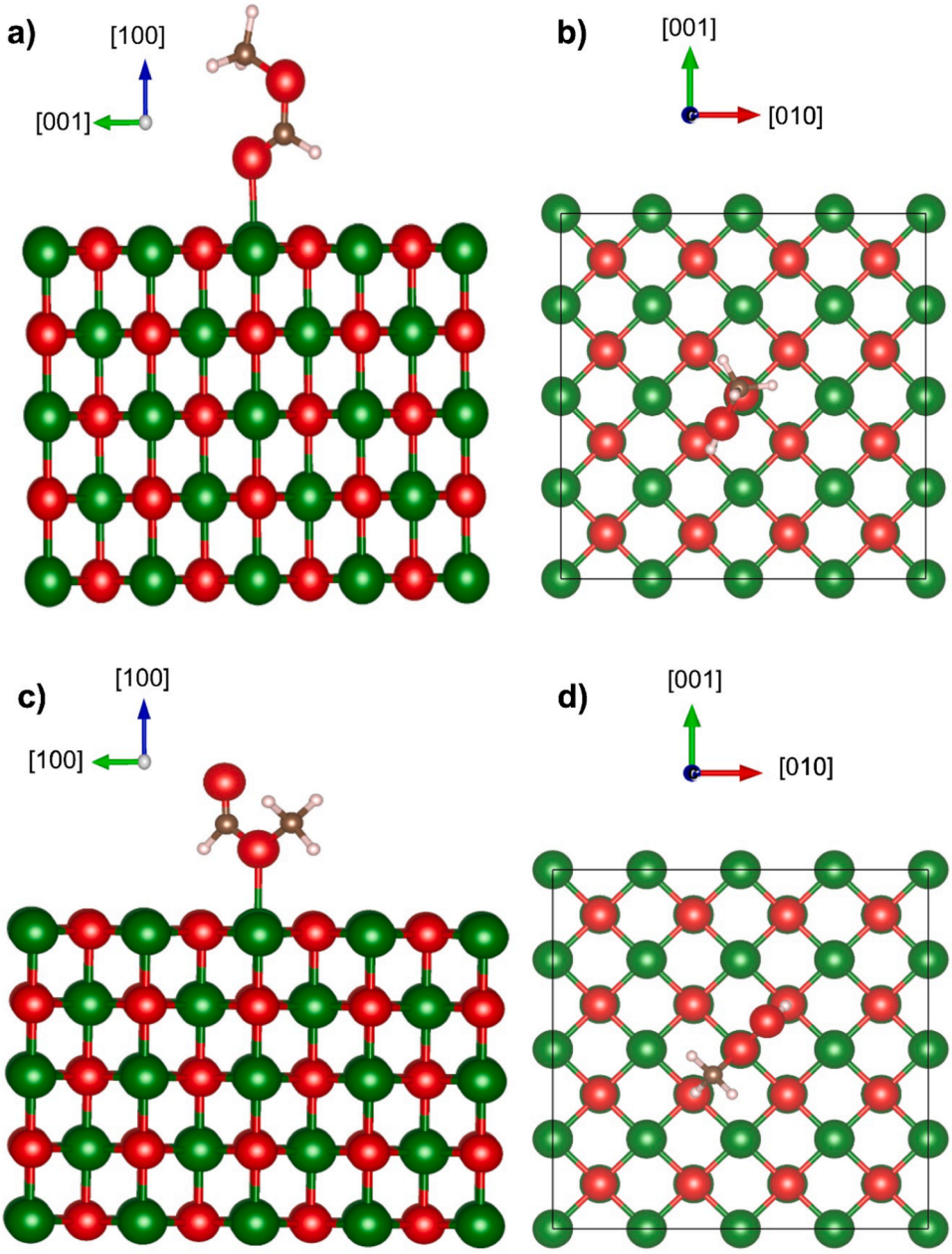


Fig. 3. Side (left) and Top (right) views of the optimized structures for the adsorbed methyl formate on MgO (100) surface; (a) Configuration 1 and (b) Configuration 2. Green, red, brown and white spheres represent Mg, O, C and H atoms respectively.

these chemical interactions is based on DOS and PDOS.

Table 1 shows the main bond distances for the molecule and surface before and after adsorption.

In the case of the methyl formate, configuration 1, slight changes are observed in the C1-H1, C1-Om1 and C1-Om2 bonds of approximately 1 % in absolute value, which correspond to the bonds of the ester group. In configuration 2, this slight bond length modification is only evident in the C1-Om2 bond. This suggests that the methyl group does not undergo significant alterations to most of the bonds following interaction with the surface. The angles O—C-O and O—C-H of the functional group change approximately 1° and between 1° and 3° respectively. The C1-Om1 and C1-Om2 values are in well concordance with previous DFT calculations of ethyl formate before the adsorption, with values of 1.22 and 1.35 Å, respectively [44].

With respect to the surface bond distances in the region close to the adsorption site, the most significant changes are observed in the Mg-O bonds of the Mg1 atom in interaction with a molecular oxygen. The Mg1-Om1 distance is 2.23 Å, which is close to the MgO distance in the perfect solid (2.10 Å) [76]. The Mg1-Om1 distance is also very close to that computed by DFT for water adsorbed on MgO (100), in which case the Mg-O(water) distance was 2.24–2.27 Å [77]. For configuration 1, the major percentage difference for these Mg-O bonds in the same surface plane is 1.91 %, while the O in the second layer is 4.81 %. Even though a similar trend occurs for both configurations, this effect is lower for configuration 2, which is probably associated with the higher physical dispersion forces that constitute the main contribution to molecule adsorption. The Mg-O bond between the molecule's oxygen atom nearest to the surface and the Mg atom is close to the value of 2.33 Å, as observed between Ca and O atom bond in the adsorption of ethyl formate on a CaO (001) surface [44]. However, in that case, there are also bonds with the other oxygen and with carbon atoms, which do not occur with methyl formate on a MgO(100) surface.

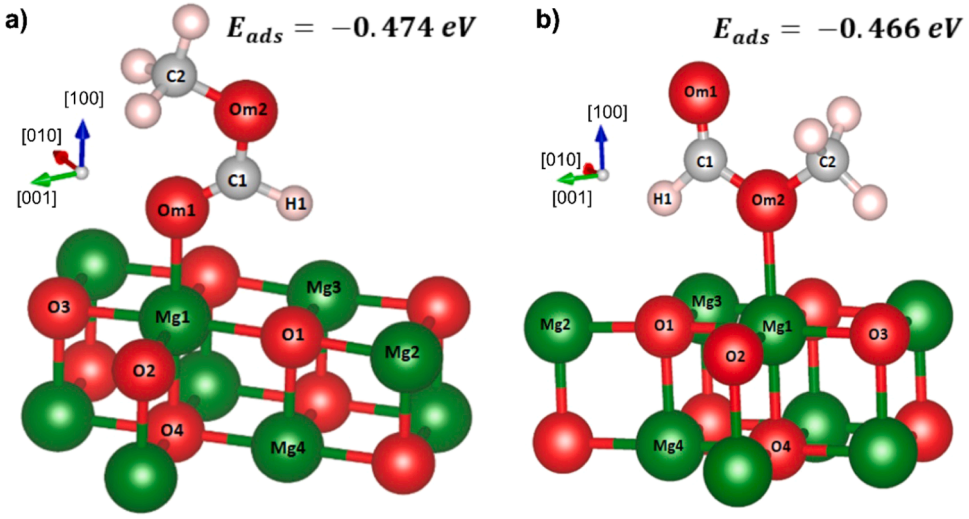


Fig. 4. Selected atoms for the methyl formate adsorbed on MgO (100) optimized structures; (a) Configuration 1 and (b) Configuration 2.

Table 1
Bond distances of methyl formate and MgO(100) surface before and after the adsorption with the respective percentage change (%Δ). The atom labels are shown on Fig. 4.

		Bond Distances/Å				
		Configuration 1			Configuration 2	
System	Bond	Before	After	% Δ	After	% Δ
MF	C1-H1	1.11	1.10	−0.90	1.11	0.00
	C1-Om1	1.21	1.22	0.83	1.21	0.00
	C1-Om2	1.35	1.34	−0.74	1.36	0.74
	Om2-C2	1.45	1.45	0.00	1.45	0.00
MgO(100)	Mg1-O1	2.09	2.13	1.91	2.11	0.96
	Mg1-O2	2.09	2.11	0.96	2.11	0.96
	Mg1-O3	2.09	2.10	0.48	2.10	0.48
	Mg1-O4(2nd layer)	2.08	2.18	4.81	2.15	3.37
	O1-Mg2	2.09	2.08	−0.48	2.09	0.00
	O1-Mg3	2.09	2.10	0.48	2.10	0.48
	O1-Mg4(2nd layer)	2.13	2.14	0.47	2.14	0.47
MF/MgO (100)	Om1-Mg1	–	2.23	–	4.43	–
	Om1-O2	–	3.07	–	4.91	–
	Om2-Mg1	–	4.34	–	2.33	–
	Om2-O2	–	4.94	–	3.17	–
	H1-O1	–	2.45	–	2.33	–
	H1-Mg3	–	2.99	–	3.21	–

3.3. Electronic structure, charge distribution, and bonding analysis of the methyl formate adsorption on MgO (100)

The electronic structure was analysed in order to obtain further data regarding the participating bonds between methyl formate and the surface during the adsorption process. Fig. 5 shows the DOS of the methyl formate molecule adsorbed on the MgO surface in configuration 1, with the inclusion of the clean surface and isolated molecule TDOS curves for comparison.

Minimal changes are observed in the two main valence bands, one between −17 and −15 eV and the other between −5 and 0 eV. In the latter region, the states of both the isolated and projected MF after adsorption make a very small contribution. The band between −5 and 0 eV is dominated by O 2p states and also contribution of Mg 2 s states, corresponding to the MgO supercell containing 80 O and 80 Mg atoms (see Fig. 5(a) and 5(b)). After adsorption, all the molecular states of MF shift to lower energies (see Fig. 5(c)). Hoffmann and Nilsson et al., among others, have explained this in detail concerning molecular interactions with surfaces [78–80] and it is similar to what happens when two atoms form a bond: the resulting molecule has a lower total energy than the separate atoms. A recent article by Saini [80], explains this fact in detail in the case of surface adsorption on alloys. However, after adsorption of methyl formate, additional peaks emerge between (−25, −20) and (−15, −5) and at more negative energies (compare Fig. 5(a) vs 5(c)). These are attributed to shifted molecular orbitals of MF (compare Fig. 5(c) vs 5(d)).

A notable observation is the comparison of the TDOS of MgO (100) (Fig. 5(b)) with the reported TDOS of MgO(bulk) (Fig. 2(a)). This comparison reveals a significant reduction of approximately 2.5 eV in the band gap values for the clean surface. A similar trend was reported by Heo et al. [81], through both DFT and reflection electron energy loss spectroscopy (REELS) experiments. It can thus be concluded that the parameters for the calculations and the GGA approximation employed have been selected with a high degree of precision.

Fig. 6 presents the TDOS of methyl formate adsorbed on MgO (100) in configuration 2 and the PDOS of the molecule. These exhibit a trend that can be interpreted in a similar manner to that observed in configuration 1.

Fig. 6(a) shows the two main valence bands corresponding to the surface (Fig. 6(b)). These bands exhibit minor alterations following the adsorption of the molecule and are newly located in the region between −17 and 15 eV and between −5 and 0 eV comparing this surface state before and after the adsorption. This is because, after the adsorption, the region in the range of −17 and −15 eV does not exhibit a contribution of molecule states. In the case of the band between −5 and 0 eV, there is only a slight contribution of MF states (see Fig. 6(a) and 6(c)). However, small peaks related to the adsorbed methyl formate orbitals are observed in the middle of these bands, between −15 and −5 eV, and at energies lower than −20 eV (compare Fig. 6(a) vs 6(c)). Furthermore, the PDOS and TDOS of the adsorbed and isolated molecule respectively (see Figs. 6 (c) and 6(d)), indicate that the adsorbed MF states shift to lower energies, suggesting that adsorption stabilizes the molecule.

Additionally, Fig. 7 shows the PDOS on the Om1 and Mg atomic orbitals of the methyl formate and MgO surface, respectively, before and after the adsorption for configuration 1, to detect finer modifications of the closest and probably bonded atoms.

For configuration 1, the PDOS on the methyl formate O atom (Om1) in the gas phase is shown in Fig. 7(a), which can be compared with the projected DOS on the same atom after the adsorption (Fig. 7(b)). The electronic structure of the isolated molecule and the adsorbed one contain sharp peaks extending in the range between −23 eV and 5 eV. These localized peaks are attributed to the discrete nature of the

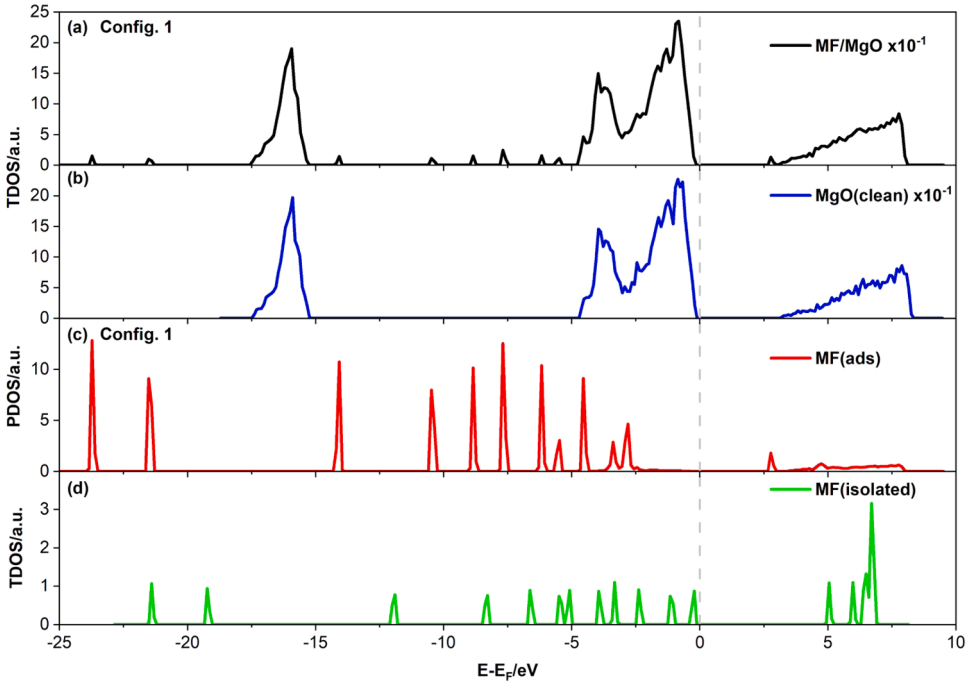


Fig. 5. DOS comparison of MF (configuration 1) adsorbed on MgO (100) surface with the clean surface and isolated molecule; (a) MF adsorbed on MgO surface TDOS, (b) MgO clean surface TDOS, (c) adsorbed MF PDOS and (d) isolated MF TDOS.

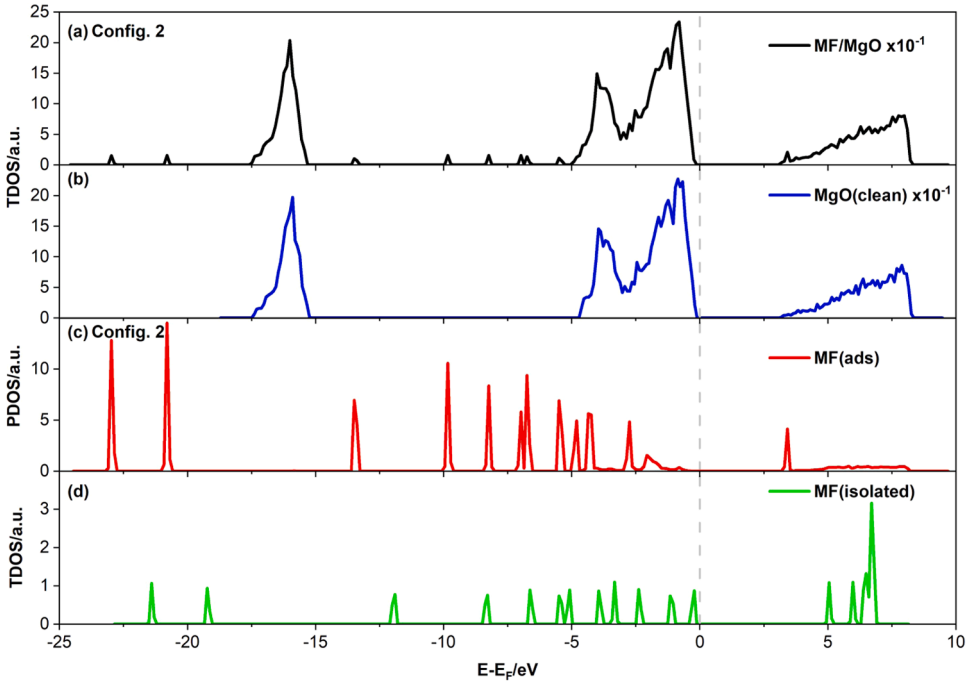


Fig. 6. DOS comparison of MF (configuration 2) adsorbed on the MgO (100) surface with the clean surface and isolated molecule; (a) MF adsorbed on MgO surface TDOS, (b) MgO clean surface TDOS, (c) adsorbed MF PDOS and (d) isolated MF TDOS.

molecule's states and are dominated by O p states and some hybridized O sp states. A comparison of the energy values of these projected states before and after adsorption reveals a general shift to the lower energy of p and s states, indicating adsorbate stabilization. Additionally, the O p states of the adsorbed methyl formate exhibit a slightly broader appearance.

The figure also presents the PDOS on the Mg atom interacting with the O atom of the methyl formate, before and after the adsorption (Fig. 7(c) and Fig. 7(d)). The band between −5 and 0 eV exhibits different features after adsorption, with three new peaks emerging that correspond to s and p states in the range between −10 and −5 eV and at approximately −2.5 eV, indicating an interaction with the molecule.

The same type of PDOS curves were obtained for the MF adsorbed on MgO surface in configuration 2, which are shown in Fig. 8.

A similar analysis can be performed for configuration 2 by calculating the PDOS on the methyl formate O atom in the gas and adsorbed

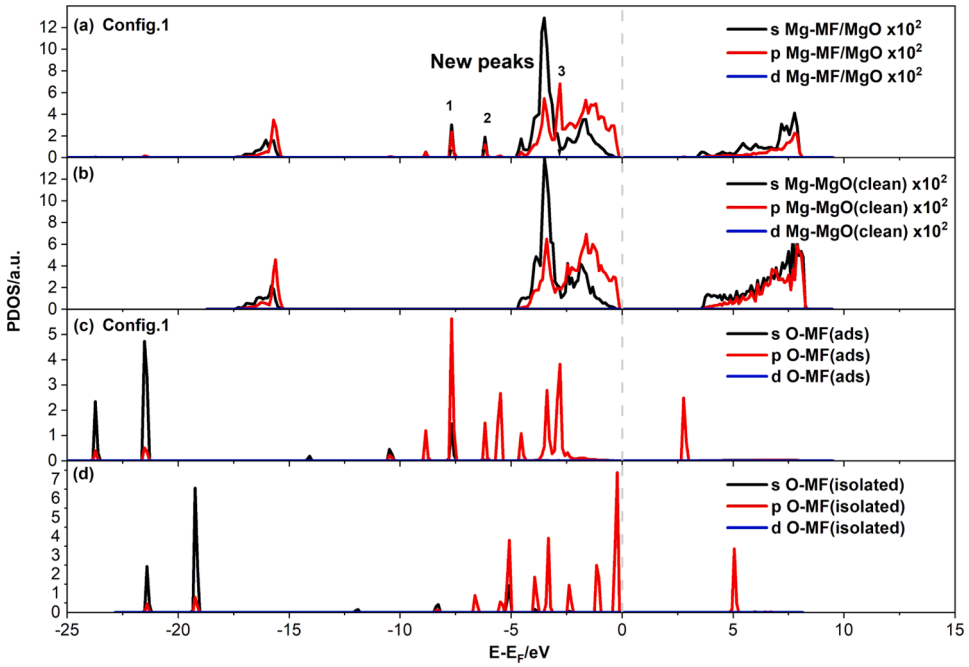


Fig. 7. PDOS on orbitals comparison between MF (configuration 1) adsorbed on the MgO (100) surface, the clean surface and the isolated molecule; (a) surface with adsorbed molecule (b) isolated surface, (c) adsorbed molecule and (d) isolated molecule.

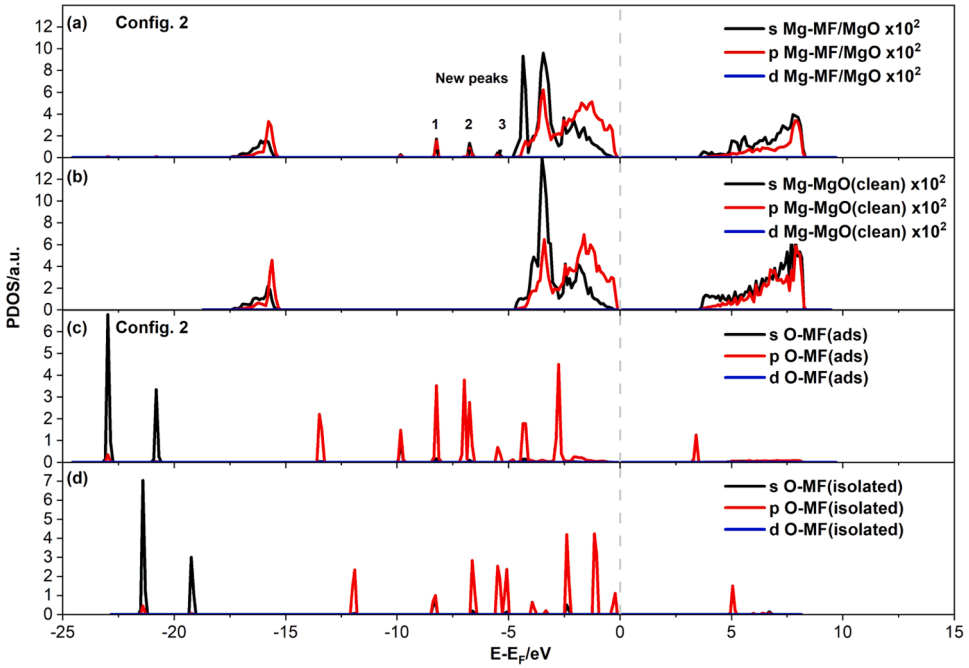


Fig. 8. PDOS on orbitals comparison of MF (configuration 2) adsorbed on MgO (100) surface with the clean surface and isolated molecule; (a) surface with adsorbed molecule (b) isolated surface, (c) adsorbed molecule and (d) isolated molecule.

phases, as well as for the Mg atom interacting with it for the clean and the surface with adsorbate.

In this configuration the O atom used for the molecule is the Om2 atom (see Fig. 4 for reference). Notably, a shift to lower energies is observed for the O p and s states of methyl formate upon adsorption, indicating enhanced chemical stability. Additionally, the emergence of three new peaks corresponding to Mg s and p states, situated within the range of −10 to −5 eV after adsorption, is evident. The distortion of the band between −5 and 0 eV is also apparent.

Furthermore, a reduction of the states of the surface conduction band after adsorption is observed, which is consistent with a charge transfer, suggesting a slightly higher charge transfer for configuration 1, which is indicative of a higher chemical interaction in this case. The d states in both configurations exhibit no significant changes, as evident in Figs. 7 and 8 (blue curve).

The following results present the Bader charges and population analysis for the atoms previously described, in accordance with geometry-based criteria. These criteria are optimal for the analysis of the electronic structure and bonding within the systems. Table 2 shows the Bader charges for these atoms.

Table 2
Net Bader charges before and after the adsorption for configurations 1 and 2. Negative and positive values indicate excess and deficiency of electrons respectively. Δ represents the absolute variation (after-before).

		Configuration 1		Configuration 2	
Atom	**Before /e**	**After/e**	**Δ/e**	**After/e**	**Δ/e**
H1	0.09	0.08	−0.01	0.08	−0.01
Om1	−1.08	−1.13	−0.05	−0.90	0.19
Om2	−1.04	−0.88	0.16	−1.07	−0.04
C1	1.50	1.33	−0.17	1.29	−0.21
Mg1	1.78	1.68	−0.10	1.75	−0.03
Mg2	1.78	1.74	−0.04	1.73	−0.05
O1	−1.78	−1.68	0.10	−1.72	0.06
O2	−1.78	−1.72	0.06	−1.73	0.05
Mg4 (2nd layer)	1.79	1.72	−0.07	1.75	−0.04
O3(2nd layer)	−1.79	−1.70	0.09	−1.72	0.07

The analysis of the Bader charge results for the atoms involved in the bonding of methyl formate with the MgO (100) surface indicates that the surface atoms closest to the molecule undergo a slight reduction in the positive charge of Mg and negative charge of oxygen atoms. The absolute maximum variation observed is approximately 0.1 for configuration 1 and 0.06 for configuration 2. In the case of methyl formate, there is a negligible increase in the negative charge of the oxygen atom in proximity to the Mg atom (Om1 for configuration 1 and Om2 for configuration 2). However, the charge is distributed along the molecule due to the O atom, which does not interact directly with the surface, and the C atom of the ester group experiences changes of approximately 0.2 e in absolute value.

Beyond this specific behavior, the evaluation of the net charge transfer to the molecule indicates a negligible net electron transfer from the surface to the adsorbate for both configurations, suggesting a low basicity of the surface. This charge transfer is −0.03 e and −0.07 e for configurations 1 and 2 respectively. Thus, these values contrast to previous results of the adsorption of ethyl formate with CaO (001) which are in the order −0.16 e and −0.13 e [44]. These differences are related with the fact that CaO surface basicity is higher than MgO. These results imply the occurrence of some electronic redistribution due to the interaction between methyl formate and the MgO (100) surface, indicating the presence of a chemical interaction in the adsorption process, albeit a weak one.

Table 3
OP values of methyl formate and MgO(100) surface before and after the adsorption with the respective percentage change (%Δ). The atom labels are shown on Fig. 4.

		OP				
		Configuration 1			Configuration 2	
System	**Bond**	**Before**	**After**	**% Δ**	**After**	**% Δ**
MF	**C1-H1**	0.558	0.613	10	0.597	7
	C1-Om1	1.207	1.154	−4	1.337	11
	C1-Om2	0.834	0.902	8	0.833	0
	Om2-C2	0.723	0.649	−10	0.667	−8
MgO(100)	**Mg1-O1**	0.161	0.152	−5	0.139	−14
	Mg1-O2	0.161	0.159	−1	0.141	−12
	Mg1-O3	0.161	0.166	3	0.139	−14
	Mg1-O4(2nd layer)	0.140	0.123	−12	0.126	−10
	O1-Mg2	0.161	0.168	4	0.164	2
	O1-Mg3	0.161	0.166	3	0.160	0
	O1-Mg4(2nd layer)	0.127	0.131	3	0.126	−1
MF/MgO (100)	**Om1-Mg1**	–	0.096	–	0.000	–
	Om1-O2	–	0.050	–	0.001	–
	Om2-Mg1	–	0.000	–	0.079	–
	Om2-O2	–	0.001	–	0.034	–
	H1-O1	–	0.072	–	0.080	–
	H1-Mg3	–	0.020	–	0.009	–

Table 3 presents the results obtained of the OP values for the molecule and surface in selected atoms before and after their interaction, with the resulting percentage variation for both most stable configurations.

A thorough examination of the OP values of the adsorbed methyl formate reveals that the primary chemical interaction between the molecule and the surface is initiated through the interaction between one of the O atoms of the molecule and the Mg1 atom, with the O atom of the molecule positioned on top of the Mg1 atom. In configuration 1, the O atom of methyl formate that interacts with the surface through Mg1 is Om1. Secondly, a weak interaction is observed between the H atom (H1) of the ester group and one of the surface oxygen atoms (O1), which is the first neighbor of the Mg1 atom. In configuration 2, methyl formate interacts with the surface, forming two main bonds of equal OP magnitude between Om2 and Mg1 atoms and H1 and surface O1 atoms. This type of interaction can be identified as a bidentate interaction, which differences from the monodentate adsorption observed for configuration 1.

These interactions result in changes to both the adsorbate and the surface, which can be identified by analyzing the OP values between the selected pair of atoms. There is a variation in the bond OP between the Mg attached to the molecule (Mg1) with their first neighbors O atoms, which is higher for the O atom in the second layer (O4) than the ones on the same plane for configuration 1, while the opposite occurs for configuration 2.

Additionally, less significant changes were observed in the Mg-O bond OP between the O1 and their first neighbors Mg atoms, indicating that the electronic distortion effect of the interaction between the molecule and the surface dissipates rapidly with increasing distance from the adsorption region. Concerning the molecule, there were some changes observed in the C—H and C—O bonds of the ester group, as well as in the C—O bond between the ester and the methyl group, for both configurations. However, in contrast to the expected result for configuration 2, the C—O bond of the ester group belonging to the O atom interacting with the surface (C1-Om2 bond) does not exhibit a variation in the OP value following interaction with the surface.

It is evident from the aforementioned changes that a chemical interaction exists between the methyl formate and the surface, albeit in a weak manner. A significantly stronger interaction was reported for ethyl formate on CaO, which can be attributed to the higher basicity of CaO compared with MgO [44].

In a similar manner to the analysis performed with the OP between selected pairs of atoms before and after the methyl formate adsorption, BO was also evaluated. The results obtained are summarized in Table 4.

A similar trend is observed, with higher BO values between the molecule Om1 atom and the Mg1 atom, constituting the main interaction. In addition, for configuration 1, the second most relevant interaction is the H1-O1 interaction, while in the case of configuration 2, both bonds (Om2-Mg1 and H1-O1), contribute practically the same magnitude. Furthermore, for the surface atoms, the variation in BO values of the bonds between the Mg1 atom and their O first neighbor atoms is observed, exhibiting a consistent tendency with the OP values. In this case, configuration 2 is found to be successful in achieving the expected outcome, characterized by a variation in the BO of the C1-Om2 bond after the interaction with methyl formate. Notably, Om2 is identified as the atom that interacts with Mg1 in this configuration. Beyond this, and that obviously, the values are not the same, it is possible to affirm a correlated change behavior on OP and BO values during the adsorption process, which represents the overlap between atomic orbitals and the strength of the formed bond respectively, relating the nature of the bond with overlapping orbitals.

Fig. 9 presents the electron density charge difference ($\Delta\rho$) of methyl formate on the MgO (100) surface for both most stable configurations.

Fig. 9 shows the electron accumulation between the O atom of the molecule close to the surface and the Mg atom below it, demonstrating the bond between these two atoms as previously mentioned. The

Table 4
BO values of methyl formate and MgO (100) surface before and after the adsorption with the respective percentage change (%Δ). The atom labels are shown on Fig. 4.

		BO				
		Config. 1			Config.2	
System	Bond	Before	After	% Δ	After	% Δ
MF	C1-H1	0.873	0.907	4	0.889	2
	C1-Om1	2.019	1.844	−9	2.202	9
	C1-Om2	1.305	1.359	4	1.249	−4
	Om2-C2	1.094	0.959	−12	0.960	−12
MgO(100)	Mg1-O1	0.201	0.181	−10	0.163	−19
	Mg1-O2	0.201	0.193	−4	0.168	−16
	Mg1-O3	0.201	0.202	1	0.164	−18
	Mg1-O4(2nd layer)	0.168	0.145	−14	0.149	−11
	O1-Mg2	0.201	0.203	1	0.200	0
	O1-Mg3	0.201	0.207	3	0.196	−2
	O1-Mg4(2nd layer)	0.153	0.156	2	0.148	−3
MF/MgO (100)	Om1-Mg1	–	0.119	–	0.005	–
	Om1-O2	–	0.054	–	0.012	–
	Om2-Mg1	–	0.002	–	0.092	–
	Om2-O2	–	0.005	–	0.034	–
	H1-O1	–	0.090	–	0.094	–
	H1-Mg3	–	0.023	–	0.013	–

positive Mg atom is surrounded by O atoms with a greater negative charge in comparison to that observed on the clean surface in the first layer. This effect is more pronounced in configuration 1. The charge distribution rapidly approaches that of the clean surface around the adsorption site, as evidenced by the Bader method. The accumulation of electrons on the Mg-O(molecule) bond confirms the covalent character over the ionic one, as was suggested by the population analysis.

Another point to consider is that the -CH_3 of configuration 1 does not experiment with any change, but in configuration 2 it is observed a variation in the C—H bond of this group. This is because in configuration in configuration 1 the methyl group does not interact with the surface (OP values are zero up to the third decimal). However, this is different for the -CH_3 group of configuration 2, where its C atom interacts with the closest oxygen of the surface (OP 0.02) and especially the H atom of this group interacts with the surface oxygen atom locating top of it (OP 0.07). These overlaps between atom orbitals are lower than the main interactions described previously, but there are enough to modify the electronic density of the molecule.

4. Conclusions

A DFT study was performed on the MgO (100) surface to investigate the adsorption of methyl formate. Adsorption energy and geometry confirm that two configurations are the most stable. Both interact through atoms belonging to the ester group or in the vicinity of it. The type of adsorption interactions can be classified as physical and chemical, with a significant contribution to the potential energy from the chemical electronic interaction and Van der Waals forces. Even though both configurations yielded a stable −0.47 eV adsorption energy, the mechanisms that stabilize the adsorption process differ. Configuration 1 is stabilized by electronic (51 %) and dispersion (49 %) interactions, while Configuration 2 is dominated by dispersion forces, contributing 73 % to the adsorption energy. These results demonstrate that while the adsorption of methyl formate is stable, its activation by the MgO stable (100) surface is challenging and likely requires defects for this purpose. Additionally, the lower adsorption energy values obtained for MgO compared to those obtained by CaO are attributable to the lower basicity of the MgO surface.

The electronic structure reveals peaks of the TDOS for the adsorption system that can be related to the adsorbed methyl formate and the surface. Within PDOS, the shift to lower energies of the molecule states after the adsorption was confirmed, which is considered to be a system stabilizing effect because of the chemical interactions between the MF and the surface for both configurations. Additionally, the reduction of states in the conduction band after the adsorption is compatible with a charge transfer from the surface to the molecule. The magnitude of this charge transfer, as evaluated using the Bader method is found to be small, in the order of 0.1 and 0.2 e, which is consistent with the low basicity of the MgO surface. Consequently, the ionic character of the bond is found to be very poor, yet some chemical interaction can be inferred.

The PDOS on site analysis shows that the molecule interacts mostly through O p orbitals with the surface, with these p orbitals close to the Fermi level being the more reactive. The Mg atom shows new peaks linked to sp hybridized orbitals, while the d orbitals do not affect the adsorption process. Finally, a bonding analysis was done to confirm the bonds seen in the geometry structure. The overlap of orbitals was found to be key to bond strength, as evidenced by the similarity of OP and BO values trend. This was further confirmed by observing bonds on charge density difference isosurfaces.

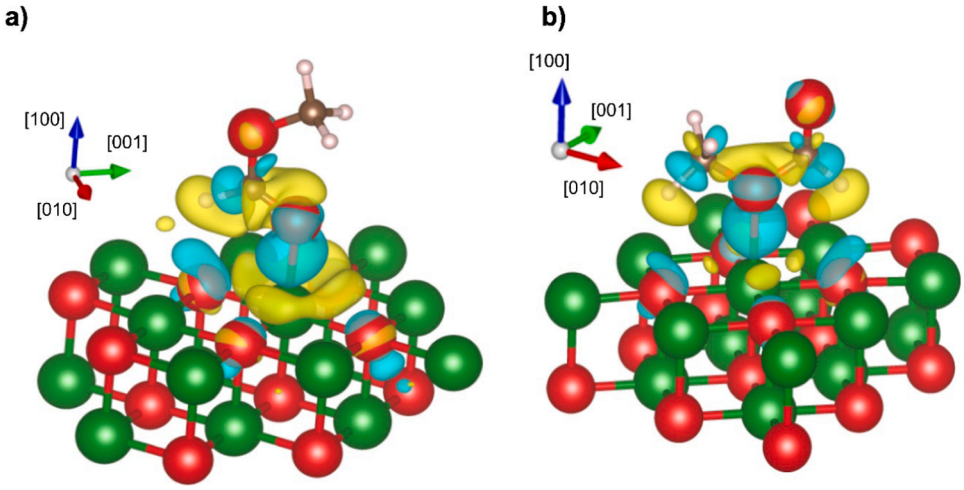


Fig. 9. Charge density difference isosurfaces with a 0.006 e/ Å^3 isovalue for MF/MgO(100) systems; (a) configuration 1, (b) configuration 2. The turquoise and yellow colors represent negative and positive charge regions respectively.

CRediT authorship contribution statement

R.E. Ambrusi: Writing – original draft, Validation, Methodology, Formal analysis, Data curation, Conceptualization. **J. Juan:** Writing – original draft, Visualization, Validation, Software, Methodology, Formal analysis, Data curation. **J.M. Marchetti:** Writing – review & editing, Supervision, Software, Project administration, Funding acquisition.

Declaration of competing interest

The authors declare that they have no known competing financial interests or personal relationships that could have appeared to influence the work reported in this paper.

Acknowledgments

Our work was supported by Universidad Nacional del Sur (UNS) and by ANPCyT through PGI-UNS 24/F083, PICT-2019–3491 and PICT-2021-I-A-01144 research grants. The simulations were performed using resources provided by UNINETT Sigma2 - the National Infrastructure for High Performance Computing and Data Storage in Norway. Dr. R.E. Ambrusi is a member of CONICET. J. Juan is a fellow researcher at CONICET. NMBU financial support to conduct this research is highly appreciated. The work was funded by EU project UNPRECENDENTED HORIZON-MSCA-2021-SE-01–01, project number 101086363. We are grateful for the suggestions of Dr. A. Juan and Dr. P. Bechthold, which contributed to the development of the quality of this work.

Supplementary materials

Supplementary material associated with this article can be found, in the online version, at doi:10.1016/j.apsadv.2025.100794.

Data availability

Data will be made available on request.

References

[1] Q. Dai, D. He, F. Meng, P. Liu, X. Liu, Dielectric constant, dielectric loss and thermal conductivity of Si3N4 ceramics by hot pressing with CeO2–MgO as sintering aid, Mater. Sci. Semicond. Process. 121 (2021) 105409, https://doi.org/10.1016/j.mssp.2020.105409.
[2] M.J. Haque, M.S. Mostari, S.B.R. Ankur, M.S. Rahman, Enhanced dielectric, ferroelectric and optical properties of Ba(Zr0.15Ti0.85)O3 ceramics incorporated with MgO, Results Mater. 10 (2021) 100176. https://doi.org/10.1016/j.rinma.2021.100176.
[3] S.M. Naga, M. Sayed, M.M. El-Omla, A.R. Wassel, N. El-Mehalawy, Processing of electric ceramic insulators from slate rocks and MgO, Mater. Manuf. Process. 35 (2020) 893–900, https://doi.org/10.1080/10426914.2020.1743853.
[4] X. Zhou, X. Ning, X. Zhang, D. Xia, B. Tang, S. Zhang, Influence of Li2O–MgO–ZnO–B2O3–SiO2 glass doping on the microwave dielectric properties and sintering temperature of Li3Mg2NbO6 ceramics, J. Mater. Sci. Mater. Electron. 31 (2020) 17029–17035, https://doi.org/10.1007/s10854-020-04260-3.
[5] R. Das, J. Shah, S. Sharma, P.B. Sharma, R.K. Kotnala, Electricity generation by splitting of water from hydroelectric cell: an alternative to solar cell and fuel cell, Int. J. Energy Res. 44 (2020) 1–24, https://doi.org/10.1002/er.5698.
[6] J.I. Di Cosimo, V.K. Diez, C.R. Apestegula, Base catalysis for the synthesis of alfa, beta-unsaturated ketones from the vapor-phase aldol condensation of acetone (1996).
[7] V.K. Díez, C.A. Ferretti, P.A. Torresi, C.R. Apesteguía, J.I. Di Cosimo, Effect of MgO activation conditions on its catalytic properties for base-catalyzed reactions, Catal. Today. 173 (2011) 21–27, https://doi.org/10.1016/j.cattod.2011.02.060.
[8] V.K. Díez, C.R. Apesteguía, J.I. Di Cosimo, Acid-base properties and active site requirements for elimination reactions on alkali-promoted MgO catalysts (2000).
[9] T. Ito, T. Tashiro, M. Kawasaki, T. Watanabe, K. Toi, H. Kobayash, Adsorption of methane on magnesium oxide studied by temperature-programmed desorption and ab initio molecular orbital methods, J. Phys. Chem. 95 (1991) 4476–4483.
[10] M.M. Branda, R.M. Ferullo, P.G. Belelli, N.J. Castellani, Methanol adsorption on magnesium oxide surface with defects: a DFT study, Surf. Sci. 527 (2003) 89–99, https://doi.org/10.1016/S0039-6028(03)00010-4.
[11] S. Peranginangin, H.B. Sembiring, Y.V.M. Nainggolan, N.S. Sihotang, H. Wijoyo, Fatty acid methyl ester (FAME) production from sludge solid waste as K2O/SiO2 catalyst, Case Stud, Chem. Environ. Eng. 10 (2024) 100933, https://doi.org/10.1016/j.cscee.2024.100933.
[12] V. Kampars, R. Kampare, A. Krumina, MgO catalysts for FAME synthesis prepared using PEG surfactant during precipitation and calcination, Catalysts 12 (2022) 226, https://doi.org/10.3390/catal12020226.
[13] B.A. Abdulkadir, A. Ramli, L.J. Wei, Y. Uemura, Effect of MgO loading on the production of biodiesel from Jatropha oil in the presence of MgO/MCM-22 catalyst, J. Japan Inst. Energy. 97 (2018) 191–199, https://doi.org/10.3775/jie.97.191.
[14] L. Meher, D. Sagar, S. Naik, Technical aspects of biodiesel production by transesterification—A review, Renew Sust Energ Rev 10 (2006) 248–268, https://doi.org/10.1016/j.rser.2004.09.002.
[15] F. Ma, M. Hanna, Biodiesel production: a review, Bioresour. Technol. 70 (1999) 1–15, https://doi.org/10.1016/S0960-8524(99)00025-5.
[16] S. Singh, D. Singh, Biodiesel production through the use of different sources and characterization of oils and their esters as the substitute of diesel: a review, Renew Sust Energ Rev 14 (2010) 200–216, https://doi.org/10.1016/j.rser.2009.07.017.
[17] Author. 2030 climate and energy framework, https://climate.ec.europa.eu/eu-action/climate-strategies-targets/2030-climate-targets_en, (n.d.). https://climate.ec.europa.eu/eu-action/climate-strategies-targets/2030-climate-targets_en.
[18] European green deal, https://commission.europa.eu/strategy-and-policy/priorities-2019-2024/european-green-deal_en, (n.d.). https://commission.europa.eu/strategy-and-policy/priorities-2019-2024/european-green-deal_en.
[19] L. Meher, V. Dharmagadda, S. Naik, Optimization of alkali-catalyzed transesterification of Pongamia pinnata oil for production of biodiesel, Bioresour. Technol. 97 (2006) 1392–1397, https://doi.org/10.1016/j.biortech.2005.07.003.
[20] A.B. Fadhil, L. Ali, Alkaline-catalyzed transesterification of Silurus triostegus Heckel fish oil: optimization of transesterification parameters, Renew Energ 60 (2013) 481–488, https://doi.org/10.1016/j.renene.2013.04.018.
[21] J. Marchetti, V. Miguel, A. Errazu, Possible methods for biodiesel production, Renew Sust Energ Rev 11 (2007) 1300–1311, https://doi.org/10.1016/j.rser.2005.08.006.
[22] M.E. Kibar, L. Hilal, B.T. Capa, B. Bahcivanlar, B.B. Abdeljelil, Assessment of homogeneous and heterogenous catayst in trasnesterifcaiotn reaction: a mini review, Chem Bio Eng Rev 10 (2023) 412–422, https://doi.org/10.1002/cben.202200021.
[23] P.K. Sarangi, A.K. Singh, S.V. Ganachari, D. Pengadeth, G. Mohanakrishna, T. Aminabhavi, Biobased heterogeneous renewable catalysts: production technologies, innovations, biodiesel applications and circular bioeconomy, Environ. Res. 261 (2024) 119745, https://doi.org/10.1016/j.envres.2024.119745.
[24] P. Patil, V.G. Gude, S. Pinappu, S. Deng, Transesterification kinetics of Camelina sativa oil on metal oxide catalysts under conventional and microwave heating conditions, Chem. Eng. J. 168 (2011) 1296–1300, https://doi.org/10.1016/j.cej.2011.02.030.
[25] A.P.S. Chouhan, A.K. Sarma, Modern heterogeneous catalysts for biodiesel production: a comprehensive review, Renew. Sustain. Energy Rev. 15 (2011) 4378–4399, https://doi.org/10.1016/j.rser.2011.07.112.
[26] B. Aghel, A. Gouran, E. Parandi, B. Hadi Jumeh, H. Rashidi Nodeh, Production of biodiesel from high acidity waste cooking oil using nano GO@MgO catalyst in a microreactor, Renew. Energy. 200 (2022) 294–302, https://doi.org/10.1016/j.renene.2022.09.045.
[27] P. Dharmegowda, I.Y. Muniyappa, L.M. Siddalingaiah, A.B. Suresh, C. Gowdru Chandrashekarappa, M.P. Prakash, MgO nano-catalyzed biodiesel production from waste coconut oil and fish oil using response surface methodology and grasshopper optimization, sustainability. 14 (2022) 11132. https://doi.org/10.3390/su141811132.
[28] A. Margellou, A. Koutsouki, D. Petrakis, T. Vaimakis, G. Manos, M. Kontominas, P. J. Pomonis, Enhanced production of biodiesel over MgO catalysts synthesized in the presence of Poly-vinyl-alcohol (PVA), Ind. Crops Prod. 114 (2018) 146–153, https://doi.org/10.1016/j.indcrop.2018.01.079.
[29] S.M. Farouk, A.M. Tayeb, R.M. Osman, S.M.S. Abdel-Hamid, Sustainable production of biodiesel from waste cooking oil using magnesium oxide nano catalyst: an optimization study, Sci Rep 14 (2024) 22010, https://doi.org/10.1038/s41598-024-71930-1.
[30] A. Eladeb, Magnesium oxide (MgO) as a sustainable catalyst for biodiesel production from waste cooking oil: a comparative study with KOH, Eng. Technol. Appl. Sci. Res. 14 (2024) 13751–13756, https://doi.org/10.48084/etasr.7055.
[31] M. Di Serio, R. Tesser, L. Pengmei, E. Santacesaria, Heterogeneous catalysts for biodiesel production, Energy & Fuels 22 (2008) 207–217, https://doi.org/10.1021/ef700250g.
[32] A.K. Singh, S.D. Fernando, Transesterification of soybean oil using heterogeneous catalysts, Energy and Fuels 22 (2008) 2067–2069, https://doi.org/10.1021/ef800072z.
[33] V. Gadore, S.R. Mishra, N. Yadava, G. Yadava, M. Ahmaruzzaman, Metal oxide based heterogenous catalysts for biodiesel production, Next Sustain 2 (2023) 100012, https://doi.org/10.1016/j.nxsust.2023.100012.
[34] K. Yu, J.R. Schmidt, Elucidating the crystal face- and hydration-dependent catalytic activity of hydrotalcites in biodiesel production, J. Phys. Chem. C. 115 (2011) 1887–1898, https://doi.org/10.1021/jp105849d.
[35] A.C.H. Da Silva, C.A. Kuhnen, S.C. Da Silva, E.L. Dall'Oglio, P.T. De Sousa Jr., DFT study of alkaline-catalyzed methanolysis of pentylic acid triglyceride: gas phase and solvent effects, Fuel 107 (2013) 387–393, https://doi.org/10.1016/j.fuel.2012.11.028.
[36] P.G. Belelli, C.A. Ferretti, C.R. Apesteguía, R.M. Ferullo, J.I. Di Cosimo, Glycerolysis of methyl oleate on MgO: experimental and theoretical study of the

reaction selectivity, J. Catal. 323 (2015) 132–144, https://doi.org/10.1016/j.jcat.2015.01.001.
[37] D. Cornu, H. Guesmi, G. Laugel, J.M. Krafft, H. Lauron-Pernot, On the relationship between the basicity of a surface and its ability to catalyze transesterification in liquid and gas phases: the case of MgO, Phys. Chem. Chem. Phys. 17 (2015) 14168–14176, https://doi.org/10.1039/c5cp00217f.
[38] J.I. Di Cosimo, V.K. Díez, C. Ferretti, C.R. Apesteguía, Basic catalysis on MgO: generation, characterization and catalytic properties of active sites, Catalysis 26 (2014) 1–28, https://doi.org/10.1039/9781782620037-00001.
[39] C.A. Ferretti, S. Fuente, R. Ferullo, N. Castellani, C.R. Apesteguía, J.I. Di Cosimo, Monoglyceride synthesis by glycerolysis of methyl oleate on MgO: catalytic and DFT study of the active site, Appl. Catal. A Gen 413–414 (2012) 322–331, https://doi.org/10.1016/j.apcata.2011.11.025.
[40] I.C. Man, S.G. Soriga Vasile, Theoretical aspects of methyl acetate and methanol activation on MgO(100) and (501) catalyst surfaces with application in FAME production, Appl. Surf. Sci. 392 (2017) 920–928, https://doi.org/10.1016/j.apsusc.2016.09.114.
[41] J.M. Montero, M.A. Isaacs, A.F. Lee, J.M. Lynam, K. Wilson, The surface chemistry of nanocrustalline MgO catalysts for FAME productions: an in situ XPS study of H2O, CH3OH and CH3OAc adsortion, Surf. Sci. 646 (2016) 170–178, https://doi.org/10.1016/j.susc.2015.07.011.
[42] V. Orazi, A. Juan, E.A. González, J.M. Marchetti, P.V. Jasen, DFT study of ethanol adsorption on CaO(0 0 1) surface, Appl. Surf. Sci. 500 (2020) 144254, https://doi.org/10.1016/j.apsusc.2019.144254.
[43] P. Bechthold, V. Orazi, A. Juan, J.M. Marchetti, A first-principles study of formic acid adsorption on CaO (001), Appl. Surf. Sci. 583 (2022) 152296, https://doi.org/10.1016/j.apsusc.2021.152296.
[44] P. Bechthold, J. Juan, A. Juan, J.M. Marchetti, The adsorption of ethyl formate on CaO: a DFT study, J. Phys. Chem. Solids. 185 (2024) 111780, https://doi.org/10.1016/j.jpcs.2023.111780.
[45] G. Kresse, J. Furthmüller, Efficiency of ab-initio total energy calculations for metals and semiconductors using a plane-wave basis set, Comput. Mater. Sci. 6 (1996) 15–50, https://doi.org/10.1016/0927-0256(96)00008-0.
[46] G. Kresse, J. Furthmuller, Efficient iterative schemes for ab initio total-energy calculations using a plane-wave basis set¨, Phys. Rev. B. 54 (1996) 11169–11186, https://doi.org/10.1103/PhysRevB.54.11169.
[47] P.E. Blochl, Projector augmented-wave method, Phys. Rev. B. 50 (1994) 17953–17979, https://doi.org/10.1103/PhysRevB.50.17953.
[48] G. Kresse, D. Joubert, From ultrasoft pseudopotentials to the projector augmented-wave method, Phys. Rev. B. 59 (1999) 1758–1775, https://doi.org/10.1103/PhysRevB.59.1758.
[49] J.P. Perdew, K. Burke, M. Ernzerhof, Generalized gradient approximation made simple, Phys. Rev. Lett. 77 (1996) 3865–3868.
[50] H.J. Monkhorst, J.D. Pack, Special points for Brillonin-zone integrations, Phys. Rev. B. 13 (1976) 5188–5192, https://doi.org/10.1103/PhysRevB.13.5188.
[51] W.H. Press, S.A. Teukolsky, W.T. Vetterling, B.P. Flannery, Numerical Recipes, Cambridge University Press, New York, 1986.
[52] S. Grimme, Semiempirical GGA-type density functional constructed with a long-range dispersion correction, J. Comput. Chem. 27 (2006) 1787–1799, https://doi.org/10.1002/jcc.20495.
[53] S. Tosoni, J. Sauer, Accurate quantum chemical energies for the interaction of hydrocarbons with oxide surfaces: cH4/MgO(001), Phys. Chem. Chem. Phys. (12AD) (2010) 14330–14340, https://doi.org/10.1039/C0CP01261K.
[54] R.L.H. Freire, D. Guedes-Sobrinho, A. Kiejna, D.S. J.L.F., Comparison of the performance of van der Waals dispersion functionals in the description of water and ethanol on transition metal surfaces, J. Phys. Chem. C. 122 (2018) 1577–1588, https://doi.org/10.1021/acs.jpcc.7b09749.
[55] D. Yuan, Y. Zhang, W. Ho, R. Wu, Effects of van der Waals dispersion interactions in density functional studies of adsorption, catalysis, and tribology on metals, J. Phys. Chem. C. 124 (2020) 16926–16942, https://doi.org/10.1021/acs.jpcc.0c02293.
[56] F.R. Rehak, G. Piccini, M. Alessio, J. Sauer, Including dispersion in density functional theory for adsorption on flat oxide surfaces, in metal-organic frameworks and in acidic zeolites, Phys. Chem. Chem. Phys. 22 (2020) 7577–7585.
[57] V. Orazi, R.E. Ambrusi, A. Morelli, A. Juan, J.M. Marchetti, DFT study of the stability and electronic properties of Ni-Doped defected (6,0) and (8,0) single-walled carbon nanotubes, Materials (Basel) 17 (2024) 6236, https://doi.org/10.3390/ma17246236.
[58] R.E. Ambrusi, S.G. García, M.E. Pronsato, Formation of Ag nanowires on graphite stepped surfaces . A DFT study, Appl. Surf. Sci. 324 (2015) 710–717, https://doi.org/10.1016/j.apsusc.2014.11.023.
[59] V. Orazi, R.E. Ambrusi, J.M. Marchetti, M.E. Pronsato, DFT study of the hydrogen adsorption and storage on Ni4 cluster embedded in multivacancy graphene, Int. J. Hydrogen Energy. 45 (2020) 30805–30817, https://doi.org/10.1016/j.ijhydene.2020.08.106.
[60] R.F.W. Bader, Atoms in molecules- A Quantum Theory (1990).
[61] T.A. Manz, N.G. Limas, Introducing DDEC6 atomic population analysis: part1. Charge partitioning theory and methodology, RSC Adv 6 (2016) 47771–47801, https://doi.org/10.1039/C6RA04656H.
[62] N.G. Limas, T.A. Manz, Introducing DDEC6 atomic population analysis: part2. Computed results for a wide range of periodic and nonperiodic materials†, RSC Adv 6 (2016) 45727–45747, https://doi.org/10.1039/C6RA05507A.
[63] N.G. Limas, T.A. Manz, Chargemol program for performing DDEC analysis (2016). Version 3.4.4ddec.sourceforge.net.
[64] G. Wu, J. Zhang, Y. Wu, Q. Li, K. Chou, X. Bao, Adsorption and dissociation of hydrogen on MgO surface: a first-principles study, J. Alloys Compd. 480 (2009) 788–793, https://doi.org/10.1016/j.jallcom.2009.02.086.
[65] A. Gueddim, N. Bouarissa, A. Villesuzanne, First-principles determination of structural properties of MgO, Phys. Scr. 80 (2009) 055702, https://doi.org/10.1088/0031-8949/80/05/055702.
[66] Y. Fei, Effects of temperature and composition on the bulk modulus of (Mg,Fe)O, 1999.
[67] S. Speziale, C.S. Zha, T.S. Duffy, R.J. Hemley, H.K. Mao, Quasi-hydrostatic compression of magnesium oxide to 52 GPa: implications for the pressure-volume-temperature equation of state, J. Geophys. Res. Solid Earth. 106 (2001) 515–528, https://doi.org/10.1029/2000jb900318.
[68] D.N. Zhang, L. Zhao, J.F. Wang, Y.L. Li, Electronic structures and the stability of MgO surface: density functional study, Surf. Rev. Lett. 22 (2015) 1550037, https://doi.org/10.1142/S0218625X15500377.
[69] M. Sassi, K.M. Rosso, First principles simulations of MgO(100) surface hydration at ambient conditions, Phys. Chem. Chem. Phys. 26 (2024) 2269–2276, https://doi.org/10.1039/D3CP04848A.
[70] J.A. Rodriguez, A. Maiti, Adsorption and decomposition of H2S on MgO(100), NiMgO(100), and ZnO(0001) surfaces: a first-principles density functional study, J. Phys. Chem. B. 104 (2000) 3630–3638, https://doi.org/10.1021/jp000011e.
[71] J.A. Rodriguez, T. Jirsak, A. Freitag, J.Z. Larese, A. Maiti, Interaction of SO2 with MgO(100) and Cu/MgO(100): decomposition reactions and the formation of SO3 and SO4, J. Phys. Chem. B. 104 (2000) 7439–7448, https://doi.org/10.1021/jp000806l.
[72] V.I. Avdeev, G.M. Zhidomirov, ELECTRONIC STRUCTURE AND OPTICAL PROPERTIES OF THE SURFACE F-CENTERS IN MgO: a THEORETICAL ANALYSIS BY DFT APPROACH, 2003.
[73] S. Labidi, J. Zeroual, M. Labidi, K. Klaa, R. Bensalem, Structural electronic and optical properties of MgO, CaO and SrO binary compounds: comparison study. Solid State Phenom, Trans Tech Publications Ltd, 2016, pp. 123–126, https://doi.org/10.4028/www.scientific.net/SSP.257.123.
[74] M. Dadsetani, R. Beiranvand, Optical properties of alkaline-earth metal oxides from first principles, Solid State Sci 11 (2009) 2099–2105, https://doi.org/10.1016/j.solidstatesciences.2009.08.018.
[75] R.E. Ambrusi, V. Orazi, J.M. Marchetti, A. Juan, M.E. Pronsato, Hydrogen storage by spillover on Ni4 cluster embedded in three vacancy graphene. A DFT and dynamics study, J. Phys. Chem. Solids. 167 (2022) 110706, https://doi.org/10.1016/j.jpcs.2022.110706.
[76] J.G. Smith, J. Naruse, H. Hiramatsu, D.J. Siegel, Intrinsic conductivity in magnesium-oxygen battery discharge products: mgO and MgO2, Chem. Mater. 29 (2017) 3152–3163, https://doi.org/10.1021/acs.chemmater.7b00217.
[77] B. Li, H. Chen, J. Feng, Q. Ma, J. Chen, B. Ren, S. Yin, P. Jiang, First principles calculation of adsorption of water on MgO (100) plane, materials (Basel). 16 (2023) 2100. https://doi.org/10.3390/ma16052100.
[78] R. Hoffmann, Solids and Surfaces: A Chemist's View of Bonding in Extended Structures, 1st ed., Wiley-VCH, 1991.
[79] A. Nilsson, L.G.M. Pettersson, Chemical Bonding at Surfaces and Interfaces, Elsevier Science, 2008, https://doi.org/10.1016/B978-0-444-52837-7.X5001-1.
[80] S. Saini, J. Halldin Stenlid, F. Abild-Pedersen, Electronic structure factors and the importance of adsorbate effects in chemisorption on surface alloys, Comput. Mater. 8 (2022), https://doi.org/10.1038/s41524-022-00846-z.
[81] S. Heo, E. Cho, H.I. Lee, G.S. Park, H.J. Kang, T. Nagatomi, P. Choi, B.D. Choi, Band gap and defect states of MgO thin films investigated using reflection electron energy loss spectroscopy, AIP Adv 5 (2015) 077167, https://doi.org/10.1063/1.4927547.